RESEARCH ARTICLE

Early detection of pulmonary vessel nodule in low dose CT image using local adaptive thresholding

Sufia Mohd Hizam, Noor Shafini Mohamad*

Centre of Medical Imaging, Faculty of Health Sciences, Universiti Teknologi MARA Cawangan Selangor Kampus Puncak Alam, 42300 Bandar Puncak Alam, Selangor, Malaysia

***Corresponding Author**

Noor Shafini Mohamad
Email: shafini.mohamad@uitm.edu.my

Abstract:

Small lung nodules are very subtle in the medical images, and less than 30% of them are connected to the pulmonary vessels. Most of the time, the findings of this disease are not optimal at the early stages. These small lung nodules have similar HU values as pulmonary vessels, therefore, making it a challenge to separate these nodules. This study aimed to segment and suppress pulmonary vessels and detected nodules to improve the accuracy of diagnosing lung cancer by using local adaptive thresholding. This proposed framework consisted of the image enhancement process and three segmentation stages. Contrast stretching, median filter combined with closing morphological operator, and unsharp masking were employed to make the image more appealing. The first stage of image segmentation was extracting lung from the parenchyma by using a fast marching method and active contour. The second stage was to extract pulmonary vessels and nodules together using local adaptive thresholding. Extraction of the nodule from the pulmonary vessels using local adaptive thresholding was employed in the final stage. The sensitivity and specificity of this method were computed by calculating the number of pixels overlapped with the ground truth images. This proposed method presented high sensitivity and specificity for segmentation of pulmonary nodule (0.90 and 0.99) and segmentation of pulmonary vessels (0.87 and 0.99). After the suppression of the vessels, the mean CNR of the nodule increased from 3.27 to 3.61). The suppression and segmentation of pulmonary vessels in CT thorax images may reduce false-positive findings and misdiagnosis due to human error. Hence, the early discovery of lung nodules can reduce about half of the mortality rate.

Keywords: Image segmentation, local adaptive thresholding, pulmonary vessel nodule

1. INTRODUCTION

According to the World Health Organisation report in 2014, lung cancer accounted for 19.1 fatalities per 100,000 population in Malaysia [1], the second leading cause of death after breast cancer. The Global Cancer Observatory report in 2018 mentioned that the incidence of new cases was 4, 686, the number of deaths was 4,057 [2]. In the latest 5-years observations, males accounted for the most incidence rate (13.2 per 100 000) compared to females (5.9 per 100 000) [3]. [1]. The gold standard of lung cancer screening tests for high-risk populations to detect at an early stage recommended by the Ministry of Health Malaysia [4] is low-dose computed tomography (LDCT). Due to inadequate participation from the public at large, a population-based screening test is not fully implemented yet [5]. Besides that, this disease is only detected when it has progressed, and most patients in Malaysia are identified with an advanced stage of cancer [4].

CT scan creates numerous cross-sectional slices, and the radiologist interprets these slices every day. By doing so in a repeated manner, it can cause exhaustion and unable to focus, thus may increase the chance of imprecise lung cancer detection and diagnosis due to human observation error [6]. Consequently, a Computer-Aided Diagnosis (CAD) system was introduced to solve this problem by assisting radiologists in making accurate reports on the findings. In Malaysia, not hospitals have fully implement CAD in their radiology department to diagnose cancers. In some cases, CAD may be too expensive and take time to learn and train radiologists to adopt this unfamiliar technology [7]. Therefore, Malaysia radiologists will depend on their visual evaluation to diagnose cancer. This situation can cause misdiagnosis because of factors linked to imaging quality and human error owing to appearance structural [8].

Li *et al.*, as cited by Gu et al. (2019), specified that pulmonary nodules are very subtle in the medical images. Less than 30% of them are connected to the pulmonary vessels, which makes them easily overlooked [6]. Lo et al. (2018) hold the view that these pulmonary vessels can be mistaken as nodules because they have similar CT values and cross-sectional shapes as nodules do [9]. Furthermore, Gu et al. (2019) reported that CAD's grey-level intensity thresholding tends to over-

segmented these nodules as separating the vessels from the nodules are quite a challenge [6].

Mustafa et al. (2018) stated that local adaptive technique yields a precise outcome as it reduces image noise around the edge regardless of the image was caused by reduced shading, ghosting, low resolution, and non-uniform lighting [10]. Assigning a distinct threshold for each pixel, based on the neighboring pixel in greyscale data is what local adaptive thresholding can do. There is a lack of research done to prove the capability of local adaptive thresholding in the segmentation of pulmonary vessels nodules. Therefore, this study aimed to segment and suppress pulmonary vessels to detect nodules, improving the accuracy of diagnosing lung cancer by using local adaptive thresholding in MATLAB. This alternative mechanism might assist the radiologist in the detection of lung cancer concurrently, avoiding misdiagnosis.

2. MATERIALS AND METHODS

This study was an experimental study where the early detection of pulmonary vessels nodules from 15 LDCT thorax images using local adaptive thresholding was investigated. These images were retrieved from VIA/I-ELCAP Public Access Research Database and saved to the personal laptop in DICOM format (Figure 1). The CT helical scans were collected using a slice thickness of 1.25mm at 120 kVp in a single breath-hold. It also includes the nodules annotation identified by experienced radiologists. The images size was 512 x 512 x 280 with 0.71 x 0.71 x 1.25 resolution. MATLAB R2018b was used to process the selected images in terms of image enhancement and image segmentation.

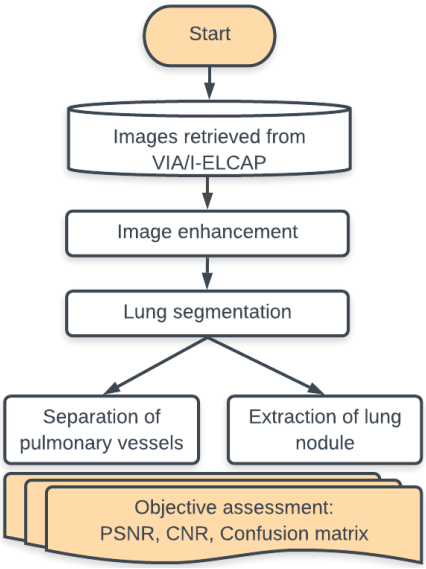

Figure 1. Research flowchart

2.1 Pre-processing steps

Most DICOM format images came out with low contrast and grainy with minimal visibility of anatomy structures. Thereby, the contrast of the image was adjusted by computing contrast stretching. This technique widened the input image has a set of pixel values to cover a more excellent dynamic range in the output image. After contrast enhancement, the low dose CT images were appeared noisy due to its low exposure settings causing insufficient photons delivered and detected. A median filter and closing morphological operator with a size 3 square structuring element were operated to remove this noise from the input images. Subsequently, the image was sharpened by using unsharp masking (Figure 2).

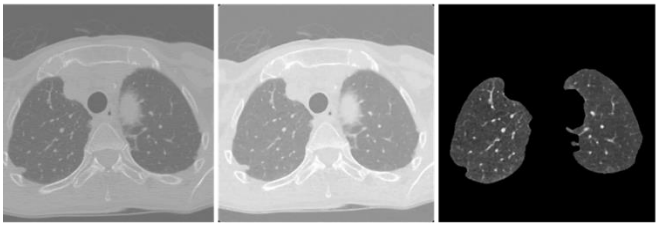

Figure 2. From left, the figure shows the original LDCT image, after the image enhancement, and the segmentation of lungs.

2.2 Image segmentation

The image segmentation framework in this paper comprised of three stages. The first stage was to obtain the lung regions from the thorax in the image by implementing a fast-marching method. Then, an active contour edge-based method was applied to get smoother edges of the lung image (Figure 2). The second stage was to segment high-intensity structures such as pulmonary vessels along with nodule attached using local adaptive thresholding (Figure 3). A sensitivity factor was chosen to a threshold as many pulmonary vessels in the image as possible. The higher the sensitivity factor, the more pixels will be selected as the foreground. For the third stage, a lower sensitivity factor than before was selected to separate the nodule from the pulmonary vessel. The nodule was extracted according to the annotation done by the radiologist in the public database. Then, dilation morphology was applied to the solitary nodule (Figure 4). As a result, two separate binary images of pulmonary vessels and pulmonary nodules alone were obtained.

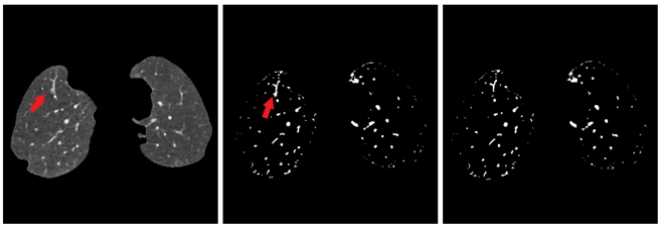

Figure 3. The image shows the segmentation of pulmonary vessels and nodules from the lung image. The red arrow points out the location of the nodule.

Figure 4. From left, a close-up image shows the nodule (red boundary by ground truth and green boundary by local adaptive thresholding) attached to the pulmonary vessels. The middle image shows the binary image. The right image displays the extracted nodule

2.3 Removal of pulmonary vessels

After the segmented pulmonary vessel image was acquired, it was subtracted with the lung image and filled the holes of the subtracted image. The next step was smoothened the lung whole region with the median filter to make it appear more natural and homogenous. The solitary nodule image was added to the lung image to make the nodule more highlighted than the surrounding parenchyma (Figure 5).

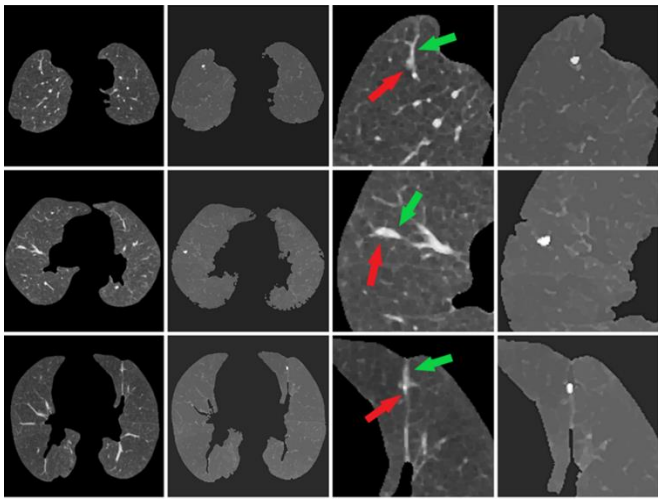

Figure 5. The left image shows the lung image before and after vessels (green arrow) suppression. Only nodule (red arrow) is preserved in the lung

2.4 Objective assessment

2.4.1 Peak Signal-to-Noise Ratio

The peak signal-to-noise ratio (PSNR) of both raw data and the pre-processed image was calculated. The PSNR results between the raw data and pre-processed images were compared using Paired T-test on SPSS. It can be expressed in decibel (dB) unit as:

$$PSNR = 10\log_{10}\left(\frac{255^2}{MSE(f,g)}\right)$$

2.4.2 Contrast-to-Noise Ratio

The contrast-to-noise ratio (CNR) of both lung image and pre-processed image were accessed, as well as the CNR nodule before and after removal of pulmonary vessels. The comparison was computed using the Paired Sample T-test in SPSS. CNR was calculated manually in decibel (dB) unit using this formula:

$$CNR = \frac{Mean\ value\ of\ object\ of\ interest\ -\ Mean\ value\ of\ background}{Standard\ deviation\ of\ background\ noise}$$

2.4.3 Confusion matrix

A confusion matrix was constructed in MATLAB to measure the performance of our method as compared to the ground truth image. Ground truth image is a gold standard that has actual outcomes. In this case, ground truth images were not available. The Otsu thresholding method was utilised to get two different masks of pulmonary vessels and nodule as ground truths. This confusion matrix consists of:

True positive (TP): the number of foreground pixels is identified as a part of both segmented image and ground truth image. **False-positive (FP):** the number of foreground pixels is identified as a part of the segmented image but are not identified in the ground truth image. **True negative (TN):** the number of negative pixels is not identified in both segmented and ground truth image (background pixels). **False-negative (FN):** the number of negative pixels is not identified in the segmented image but identified as a part of the ground truth image.

From these values, the sensitivity (TP/TP+FN), specificity (TN/TN+FP), positive predictive value (TP/TP+FP), negative predictive value (TN/TN+FN), DICE (2TP/(2TP+FP+FN)), and Jaccard (TP/(TP+FN+FP) were calculated. The sensitivity was concerned with several positive values that were detected as positive—the specificity considered on the number of negative values that were detected as negative. DICE and Jaccard were achieved to evaluate the similarity of area overlapped with the ground truth.

3. RESULTS AND DISCUSSION

Table 1 shows the mean PSNR of original images, 19.8284±0.0398, while the mean PSNR of pre-processed images was 20.4999±0.2766. There was a significant difference between the PSNR of the original image and PSNR of the pre-processed image (-0.6715, $p<0.001$). This implies that there was an increase in PSNR value when the noise removal method was applied to the original image.

The mean value of the original image CNR was -14.8771±3.8146, whereas the mean value of pre-processed image CNR was 0.2366±0.0649. There was a significant difference between the CNR of the original image and CNR of the pre-processed image (-15.1137, $p<0.001$). This indicates that there was an increase of mean CNR value when the contrast enhancement technique was applied to the images.

Table 1. The summary of the Paired Sample T-test of PSNR and CNR of the original image and PSNR of pre-processed image.

	Mean	Mean differences	Sig (2-tailed)
PSNR original	19.8284±0.0124	-0.6715	0.001
PSNR pre-processed	20.4999±0.0983		
CNR original	-14.8771±3.8146	-15.1137	0.001
CNR pre-processed	0.2366±0.0649		

The median filter can remove deviations with huge magnitudes while maintaining the degree of image edges. Thus, there is less blurring in the image. An experiment was done by Muthamil Selvi & Ashadevi (2020) on evaluating impulse and Gaussian noise suppression from CT lung images by comparing different smoothing filters has shown that the median filter had higher PSNR values than the mean and wiener filter [11]. Another study on CT lung images has been done to detect edges and denoise by using a combination of various morphological operators. The findings showed that the morphology algorithm had the highest PSNR value than Canny, Sobel, and the novel mathematic morphological algorithm [12].

Table 2 shows the CNR mean value of lung nodule with the presence of lung vessels was 3.2658±0.6992, and the CNR mean value of lung nodule without the presence of lung vessels was 3.6111±0.6515. There was a significant difference between both mean CNR values (-0.3453, p= 0.004). This suggests that there was an improvement of CNR nodule value when the lung vessels were suppressed from the lung parenchyma.

Table 2. The summary of the Paired Sample T-test of PSNR and CNR of the original image and PSNR of pre-processed image.

	Mean	Mean differences	Sig (2-tailed)
CNR nodule with vessels	3.2658±0.6992	-0.3453	0.004
CNR nodule without vessels	3.6111±0.6515		

When calculating for the nodule CNR, the background noise assigned was the lung parenchyma that included the high-intensity pulmonary vessels. This is because the background might not be entirely uniform and contain noise that resulted in low CNR (3.2658±0.6992). After the suppression of pulmonary vessels, the empty holes were filled. Consequently, the lung parenchyma became homogenous, and the nodule preserved in its location. Now, the images display pulmonary nodules, where they are the only high-intensity object presented compared to that of surrounding parenchyma (CNR=3.6111±0.6515, p= 0.004).

Gu et al. (2019) extracted pulmonary vessels from the lung parenchyma by using a two-cascaded convolutional neural network (CNN) and filled in the void with the same voxels as the parenchyma to make it looked more natural [6]. The mean CNR nodule in their study increased from 4.23 to 6.95 (39.14%). Local adaptive thresholding had an increased CNR of 9.42% (3.27 to 3.61). The two-cascaded CNN was robust and was able to extract pulmonary vessels accurately. Therefore, more natural-looking parenchyma was produced that may contain less background noise. In the current study, the 9.42% CNR improvement showed that pulmonary nodules are more highlighted when the pulmonary vessels are suppressed.

Table 3. The summary of the nodule segmentation confusion matrix.

Nodule	Sensitivity	Specificity	PPV	NPV	DICE	Jaccard
Image 1	1.00	1.00	0.78	1.00	0.88	0.78
Image 2	1.00	1.00	0.67	1.00	0.80	0.67
Image 3	0.93	0.99	0.50	0.99	0.65	0.48
Image 4	0.68	1.00	0.56	0.99	0.61	0.44
Image 5	0.79	0.99	0.68	0.99	0.73	0.58
Image 6	1.00	1.00	0.78	1.00	0.88	0.78
Image 7	1.00	0.99	0.46	1.00	0.63	0.46
Image 8	1.00	1.00	0.84	1.00	0.91	0.84
Image 9	1.00	1.00	0.79	1.00	0.88	0.79
Image 10	0.92	0.99	0.69	0.99	0.79	0.65
Image 11	0.74	0.99	0.52	1.00	0.61	0.44
Image 12	0.96	0.99	0.40	1.00	0.60	0.43
Image 13	1.00	0.99	0.72	1.00	0.84	0.72
Image 14	0.61	0.99	0.56	1.00	0.58	0.41
Image 15	0.92	0.99	0.63	0.99	0.74	0.59
Average	0.90	0.99	0.64	0.99	0.74	0.60

As stated by Pont-Tuset & Marques (2016), a small sensitivity score is the product of under-segmentation and implies the inability to detect distinctive shape [13]. Small PPV score and high false detection of object boundary pixels imply the over-segmentation technique.

Table 3 shows that local adaptive thresholding yielded a sensitivity of 90.67% in segmenting pulmonary vessel nodule. Liu et al. (2019) used a robust transition region-based thresholding to extract 50 nodules images that were attached to the pleura and compared the results with ground truth images generated by radiologists [14]. This thresholding method selected the intermediate pixels of 0.85 in between the foreground and the background region. The sensitivity of their method was 86.65%. This shows that local adaptive thresholding had high sensitivity; therefore, under-segmentation was unlikely to occur. Local adaptive thresholding was able to delineate the shape of the pulmonary nodule as close as the ground truth, even if the nodule was attached to the pulmonary vessels. This is because the local adaptive threshold manipulates a local pixel around the neighborhood instead of the whole region (Figure 4).

On the other hand, our overall PPV score was 0.64. This implies that our proposed method has average PPV; as a result, slight false detection of pulmonary vessel nodule boundary occurred. The overall specificity was 0.99. This indicates that the division between background and the pulmonary nodule was accurate [15]. The overall DICE and Jaccard score of this proposed method were ranged from 0.74 and 0.60 (Table 3).

Table 4. The summary of vessel segmentation confusion matrix.

Vessels	Sensitivity	Specificity	PPV	NPV	DICE	Jaccard
Image 1	0.86	0.99	0.64	0.99	0.73	0.58
Image 2	0.86	0.99	0.67	0.99	0.75	0.60
Image 3	0.92	0.99	0.68	0.99	0.78	0.64
Image 4	0.94	0.99	0.67	0.99	0.78	0.65
Image 5	0.98	0.99	0.68	0.99	0.80	0.67
Image 6	0.80	0.99	0.37	0.99	0.50	0.33
Image 7	0.94	0.99	0.67	0.99	0.80	0.64
Image 8	0.84	0.99	0.66	0.99	0.67	0.50
Image 9	0.94	0.99	0.73	0.99	0.82	0.69
Image 10	0.82	0.99	0.57	0.99	0.67	0.51
Image 11	0.82	0.99	0.52	0.99	0.64	0.47
Image 12	0.86	0.99	0.59	0.99	0.70	0.54
Image 13	0.81	0.99	0.40	0.99	0.53	0.36
Image 14	0.81	0.99	0.47	0.99	0.60	0.43
Image 15	0.88	0.99	0.71	0.99	0.80	0.65
Average	0.87	0.99	0.60	0.99	0.70	0.55

Regarding Table 4, the overall sensitivity of local adaptive thresholding in segmenting pulmonary vessels was 0.87, and the PPV was 0.60. A study by Zhai, Staring, & Stoel (2016) implemented graph-cuts algorithm to segment pulmonary vessels from CT images [16]. The authors enhanced the vessels with a Hessian-based filter and assigned foreground and background pixels by altering graph cuts parameters with a modified Gaussian function [16]. The graph cuts method held a sensitivity score of 0.73 and PPV of 0.79. Local adaptive thresholding had higher sensitivity; therefore, the delineation of the pulmonary vessel shape was as close as the ground truth image.

On the contrary, the overall PPV score was lower (0.60); as a result, false detection of pulmonary vessel boundary occurred. The sensitivity factor of local adaptive thresholding influences how many foreground objects are thresholded. Therefore, the higher the sensitivity factor, the more local pixels are selected to be foregrounds. Local adaptive thresholding with high sensitivity factor able to threshold more large and small pulmonary vessels as compared to ground truth image; because of that, over-segmentation of the pulmonary vessels occurred.

DICE and Jaccard assess any similarities between the predicted segmentation algorithm and the ground truth algorithm. Both metrics hold on a set of agreements in terms of 0 and 1. If the score of the overlapping area is close to 0, there is no overlapping occurs. If the score of the overlapping area is close to 1, the area in both the predicted algorithm and ground truth algorithm is said to be overlapped [13]. In this case, local adaptive thresholding yielded an overall DICE score of 0.70 and an overall Jaccard score of 0.55 in segmenting pulmonary vessels (Table 4). To appraise the effectiveness of local adaptive thresholding in segmenting pulmonary vessels, the current results were compared with Gu et al. (2019) [6]. These authors used two cascaded CNN that instantly convert with image data as information and automatically produce voxel-based attributes that separate the pulmonary vessels and pulmonary nodules from the surrounding parenchyma. [6] method yielded a higher DICE score of 0.94 and the Jaccard score of 0.89, which was lower than the current study. Local adaptive thresholding selected more pulmonary vessels as foreground pixels than the ground truth method. Consequently, more areas in the predicted segmentation image did not accurately overlap with the actual segmentation image.

4. CONCLUSION

The segmentation framework in this paper utilised local adaptive thresholding to separate the nodule from pulmonary vessels. The method presented high sensitivity and specificity score for both nodule and pulmonary vessel segmentation. Local adaptive thresholding can be an alternative tool to improve the process of segmentation of pulmonary vessels nodules that are smaller than 30mm. The suppression and segmentation of pulmonary vessels in CT thorax images may reduce false-positive findings and misdiagnosis due to human error. Hence, the early discovery of lung nodules can reduce about half of the mortality rate. Further study is recommended to apply this experiment to the clinical site to assist radiologists in decision-making. A neural network can be utilised to classify lung cancers into benign and malignant. This way, the workload can be reduced, and lung cancer can be detected early.

ACKNOWLEDGEMENTS

Authors would like to thank Dr. Noor Elaiza Abd Khalid for assistance in MATLAB protocols.

REFERENCES

[1] K. C. Siang and C. K. M. John, "A review of lung cancer research in Malaysia," *Med. J. Malaysia*, vol. 71, no. June, pp. 70–78, 2016.

[2] The Global Cancer Observatory, "Malaysia - Cancer fact sheet," *World Heal. Organ.*, vol. 593, pp. 1–2, 2019.

[3] Azizah AM. *et al.*, *Malaysia National Cancer Registry Report 2012-2016*. 2019.

[4] Malaysian Health Technology Assessment Section, "Low Dose Computed Tomography for Lung Cancer Screening," *Heal. Technol. Assess. Rep.*, p. 122, 2017.

[5] P. Rajadurai, S. H. How, C. K. Liam, A. Sachithanandan, S. Y. Soon, and L. M. Tho, "Lung Cancer in Malaysia," *J. Thorac. Oncol.*, vol. 15, no. 3, pp. 317–323, 2020.

[6] X. Gu, J. Wang, J. Zhao, and Q. Li, "Segmentation and suppression of pulmonary vessels in low-dose chest CT scans." p. 12, 2019.

[7] J. Shiraishi, Q. Li, D. Appelbaum, and K. Doi, "Computer-aided diagnosis and artificial intelligence in clinical imaging," *Semin. Nucl. Med.*, vol. 41, no. 6, pp. 449–462, 2011.

[8] A. Jalalian, S. Mashohor, R. Mahmud, B. Karasfi, M. Iqbal Saripan, and A. R. Ramli, "Computer-Assisted Diagnosis System for Breast Cancer in Computed Tomography Laser Mammography (CTLM)," *J. Digit. Imaging*, vol. 30, no. 6, pp. 796–811, 2017.

[9] S. C. B. Lo, M. T. Freedman, L. B. Gillis, C. S. White, and S. K. Mun, "Computer-aided detection of lung nodules on CT with a computerized pulmonary vessel suppressed function," *Am. J. Roentgenol.*, vol. 210, no. 3, pp. 480–488, 2018.

[10] W. A. Mustafa, H. Yazid, and M. Jaafar, "An improved sauvola approach on document images binarization," *J. Telecommun. Electron. Comput. Eng.*, vol. 10, no. 2, pp. 43–50, 2018.

[11] P. Muthamil Selvi and B. Ashadevi, "Elimination of noise in CT images of lung cancer using image pre-processing filtering techniques," *Int. J. Adv. Sci. Technol.*, vol. 29, no. 4 Special Issue, pp. 1823–1832, 2020.

[12] M. Kumar and S. Singh, "Edge Detection and Denoising Medical Image using Morphology," *Int. J. Eng. Sci. Emerg. Technol.*, vol. 2, no. 2, pp. 66–72, 2012.

[13] J. Pont-Tuset and F. Marques, "Supervised Evaluation of Image Segmentation and Object Proposal Techniques," *IEEE Trans. Pattern Anal. Mach. Intell.*, vol. 38, no. 7, pp. 1465–1478, 2016.

[14] J. Liu, J. Gong, L. Wang, X. Sun, and S. Nie, "Segmentation refinement of small-size juxta-pleural lung nodules in CT scans," *Iran. J. Radiol.*, vol. 16, no. 1, 2019.

[15] A. A. Taha and A. Hanbury, "Metrics for evaluating 3D medical image segmentation: Analysis, selection, and tool," *BMC Med. Imaging*, vol. 15, no. 1, 2015.

[16] Z. Zhai, M. Staring, and B. C. Stoel, "Lung vessel segmentation in CT images using graph-cuts," *Med. Imaging 2016 Image Process.*, vol. 9784, p. 97842K, 2016.